COLLECTIVE BEHAVIOR

Cross-link collective: Entangled robotic matter with cohesive motion

Danna Ma[1], Baxi Chong[2], Daniel I. Goldman[3], Kirstin H. Petersen[1]*

Robotic applications increasingly demand systems that are resilient, adaptable, and scalable. One promising route is through collectives of simple modules, where complex group-level behavior emerges from local interactions. By omitting fixed topologies and tight coordination, this approach sacrifices predictability and conventional tools for behaviors inherently optimized through stochastic mechanical interactions. A key challenge is maintaining cohesion and functionality without fixed connections and explicit coordination. We introduce the cross-link collective, a physically entangled robotic system inspired by cross-linking in active gels. Through shape morphing and transient entanglement, individually immobile modules produce sustained collective motion. The mechanically intelligent robot matter favors chains and phase relationships that reduce joint torques and reconfigures in response to perturbations. We show that distributed control can be added to this substrate to further enhance cohesion. Leveraging weak, reversible connections, the cross-link collective is adaptable, scalable, and fault tolerant, offering insights to applications from soft matter and robotics.

INTRODUCTION

Traditional robotic systems consist of fixed topologies and carefully coordinated interactions across sensors, actuators, and controllers. Although this approach is demonstrably powerful, relying on a preconceived notion of "good" design practices can hinder the embodied and mechanical intelligence that emerges when components are allowed to self-organize in response to their surroundings. Here, we explore how entanglement, that is, transient physical coupling of shape-morphing modules, can cause mechanical intelligence to emerge. The concept is closely inspired by natural collectives composed of stochastically interacting units that achieve capabilities, resilience, and scalability far beyond those of monolithic engineered systems.

In natural collectives, stochastic entanglement is used broadly to overcome environmental and mechanical challenges, as illustrated in Fig. 1. In some systems, it enables new collective functions: Fire ants link legs and mandibles to form temporary architectures that allow the group to cross gaps, remain afloat, and navigate complex terrain (*1*). In others, it serves to reduce environmental stress: California blackworms knot into dense, reversible aggregates that slow evaporative loss and buffer temperature gradients, improving survival under drying or cooling conditions (*2*). Entanglement can also be used to resist environmental forces: Mussels secrete byssal threads that tangle with neighbors and substrates, dissipating hydrodynamic shear and preventing dislodgement in turbulent flow (*3*). In some cases, entanglement helps to share load and maintain stability: Filamentous fungi form branching mycelium that anchors to substrates, providing long-term structural integrity against gravity and mechanical perturbations (*4*). At the molecular scale, active gels such as actomyosin networks use transient physical and chemical cross-links between filaments, which rearrange to dissipate internal shear and adapt stiffness while preserving overall mechanical integrity (*5*). Across these examples, the degree and transience of entanglement are tuned to specific environmental challenges, yet all rely on local mechanical interactions, with little or no exteroception, to achieve group-level capabilities beyond those of any individual.

Recently, these natural systems have inspired a number of modular robot-like platforms, where internal connections are formed stochastically and where globally useful properties emerge from mechanical intelligence. Prior studies typically relied on local interactions between planar circular robotic modules. Veenstra *et al.* (*6*) used modules in preconfigured chains with tunable elasticity to produce adaptive locomotion. Saintyves *et al.* (*7*) designed modular units whose torque and angular-speed parameters allowed aggregates to switch between liquid- and solid-like states, similarly yielding terrain-adaptive locomotion. However, these works offered only limited insight into dynamic self-reconfiguration and the optimality of emergent chain morphologies. Devlin *et al.* (*8*) similarly studied topological rearrangement dependent on interunit forces, and others demonstrated emergent locomotion (*9*–*11*) and aggregation (*12*, *13*) in loosely coupled magnetic modules, yet, in all cases, the behaviors arose primarily in dense aggregates and relied on global signals or preprogrammed states. Other studies have focused on morphologies that specifically induce mechanical chaining or entanglement. Savoie *et al.* (*14*) combined shape-morphing and jammed modules to achieve directed motion, albeit only within a mobile boundary that prevented diffusion of the collective. Ozkan-Aydin *et al.* (*2*) and Kaeser *et al.* (*15*) examined dense blob-like entangled collectives where individual gaits influenced overall mobility but without notable reconfiguration, chain optimization, or long-range migration. In summary, a detailed analysis of how entangled chains form and influence collective motion and cohesion remains limited.

In this Research Article, we take inspiration from these natural and engineered systems to introduce a robotic collective that behaves analogously to an active gel, stochastically forming and reconfiguring chains through local mechanical interactions (Movie 1). The system comprises simple, shape-shifting modules with limited sensing and self-locomotion, which collectively produce sustained motion even under external forces and perturbations. Owing to its entanglement-based cohesion, where each module is itself a three-link chain capable of weak or moderate coupling to others, we refer to this platform as the cross-link collective. The collective favors

[1]School of Electrical and Computer Engineering, Cornell University, 455 Hoy Road, Ithaca, NY 14853, USA. [2]Department of Mechanical Engineering, Pennsylvania State University, 226 Reber Building, University Park, PA 16802, USA. [3]School of Physics, Georgia Institute of Technology, 225 North Avenue, Atlanta, GA 30332, USA.
*Corresponding author. Email: kirstin@cornell.edu

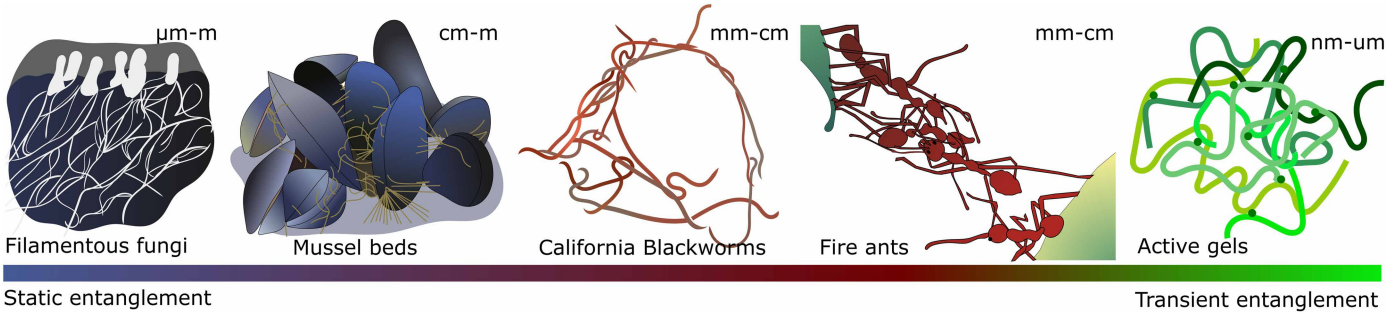

Fig. 1. Enhancing cohesion, functionality, and resilience through entanglement. From organismal to molecular scales, entangled networks in nature resist environmental stresses, have tunable mechanical properties, support collective behaviors, and form dynamic architectures. Figure created by the authors using Inkscape.

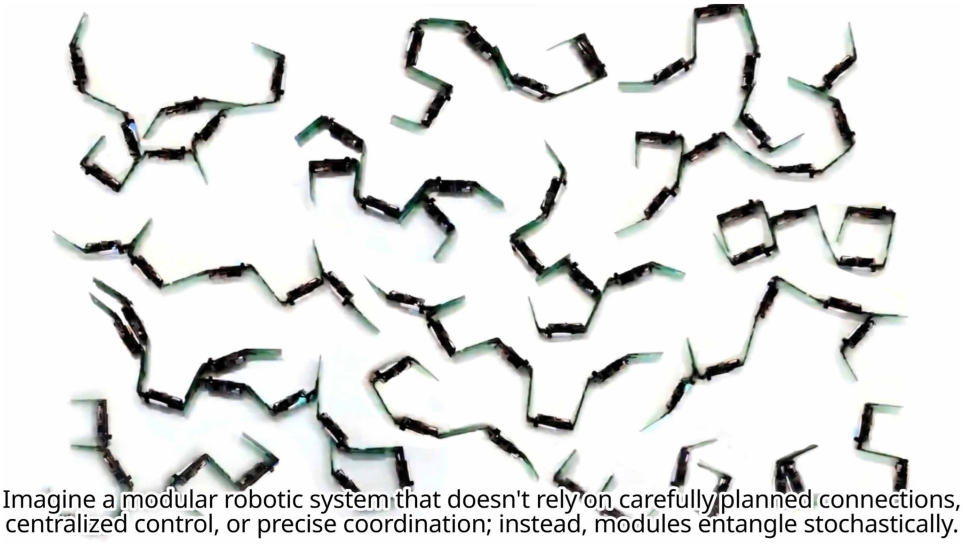

Movie 1. Overview of the article motivation, methods, and results.

elongated chain morphologies that help it maintain cohesion and adapt to external forces without centralized control, global planning, or global synchronization. Unlike systems bound by physical barriers or permanent connections, our system exhibits viscous-like yielding: Chains break under stress, allowing flow and recovery in cluttered environments. Through a combination of experimental results and comparative modeling, we show that the collective inherently promotes chain configurations with superior locomotion performance and that these chains self-regulate internal torques and phase drift. We also show that simple computational intelligence can be layered on top of this mechanically intelligent substrate to further enhance cohesion during extended, unconstrained motion. A proprioceptive controller based on low-fidelity sensors allows modules to estimate whether they are part of a chain and, if not, stall their neighbors to facilitate reattachment. This encourages local regions to behave as transient solids, enabling isolated modules to reintegrate into the collective.

A key strength of the minimalistic approach presented here is a substantial tolerance to noisy interactions, sensors, models, and faulty individuals, as well as low cost, part redundancy, and graceful degradation. Insights from this study and platform design apply to soft matter physics and programmable matter, as well as terrain adaptive robotic swarms that physically flow, reshape, and self-organize across surfaces in response to environmental cues or internal dynamics.

RESULTS

Module design and capabilities

The modules introduced in this work are three-link robotic modules inspired by Purcell's minimalistic swimmers (*16*) that oscillated between "I" (linear) and "U" (cup) shapes to interact mechanically with others. A close-up of this transformation can be seen in movie S1. These are reminiscent of the Smarticles platform, which oscillates between I and "Z" shapes and, since its first introduction in 2015 (*17*), has been leveraged for a number of studies related to emergent directed motion (*14*, *18*–*20*), biophysical models for migrating California worms (*2*), and mechanical self-organization (*21*, *22*). Whereas the original design worked well for papers focused on the emergent behavior that arises because of planar, multibody contact dynamics, it was not optimized for physical entanglement. Specifically, the outer links were driven by two rotational servos, which made the center link bulky, in turn limiting the number of simultaneous physical interactions per module and preventing a high degree of entanglement. Because the physical interactions of many Smarticles led to separation,

collective behaviors were maintained by confining them to a small fixed arena (*21*), adding a physical boundary (*14*, *19*, *22*), and/or by stapling them together (*2*).

The cross-link modules were optimized for entanglement and cohesion (*23*). The most important distinction was that the modules had only one degree of freedom: A single motor located on the center link simultaneously drove the two outer links via a worm gear coupled with a crank and slider mechanism, such that the modules could transition from an I to a U shape (Fig. 2, A and B). The low thread angle of the worm gear meant that the mechanism was not back-drivable. Therefore, although the onboard motor was relatively weak, the holding force of the modules was limited only by the point of plastic deformation on the linkages. The crank and slider mechanism facilitated a low-weight, slender module profile, which, in turn, permitted optimal geometric cohesion as defined in (*24*), in both two and three dimensions. Examples of the cross-link collective in a three-dimensional (3D) pile, suspended from a pole, and jamming/flowing through a funnel are provided in the "Module profile and entanglement properties" section of Supplementary Materials and Methods and movie S2.

The choice of the U shape was inspired by recent advances in active matter systems, as proposed in (*18*, *24*), and was motivated by our interest in entanglement and cohesion. Specifically, each individual U-shaped module maintains symmetry about its central longitudinal axis throughout the shape-changing process. At the collective level, multiple connected U-shaped modules could form traveling waves, which we found to be beneficial for locomotion. To quantify the relationship among entanglement, cohesion, and locomotion performance, our study investigated the mechanics of various chain configurations and analyzed their corresponding locomotion behaviors.

The module design directly integrated all electronic components, including a microcontroller, a battery and voltage converters, and a motor driver. The sensor modalities included a three-axis accelerometer, a battery sensor, a motor current sensor, a rotational encoder, an infrared photo transistor, and a microphone-buzzer pair for noncontact interactions (Fig. 2C). Facilitated by our choice of materials, each module weighed just 25 g and could morph between substantially different shapes: from a 200 mm–by–20 mm–by 20 mm I shape to an 80 mm–by–65 mm–by 20 mm U shape. We defined the body length (BL) of a module to be 80 mm. When orthogonal to the center link, the outer link could lift up to 3.9 other modules, and the holding strength, which persisted when the motor was off, was 41.6 other modules ("Module lifting and holding force" section of Supplementary Materials and Methods). Most critically, the length ratio of the

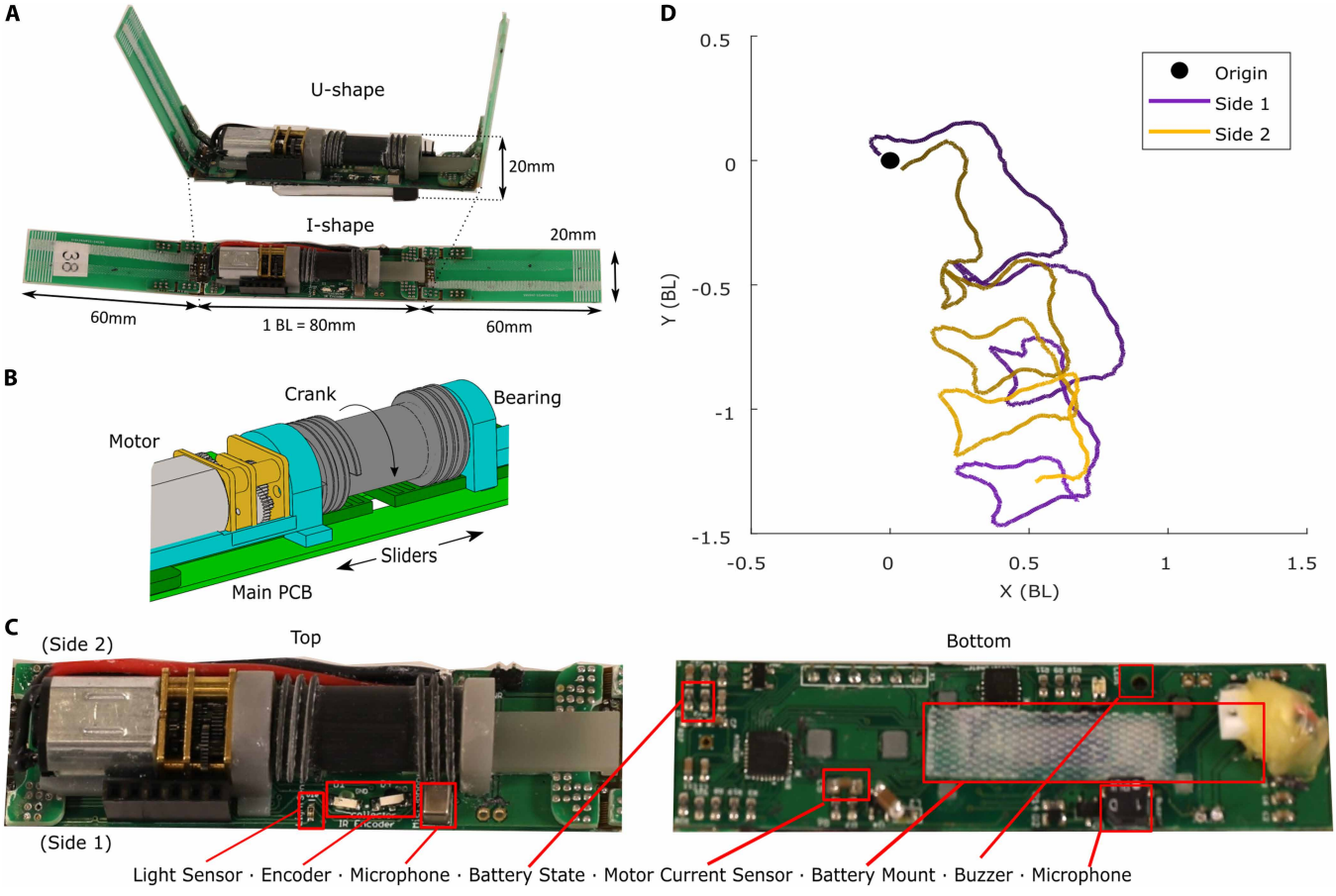

Fig. 2. Robotic modules used in this study. (**A**) Modules in U and I shapes, respectively. (**B**) Modules are composed primarily of PCBs; the wings are operated by a single motor with a worm gear that drives a crank and slider mechanism. (**C**) Module processor, power, and sensing modalities. Labels indicate the orientation of side 1 and side 2 relative to the hardware layout. (**D**) Motion trajectories of a single module resting on side 1 and side 2 over 180 oscillation cycles on a planar surface. The line shading indicates temporal evolution, fading from darker to lighter along the direction of motion.

center link to the outer links was 0.75, which falls within the optimal range for entanglement as predicted in (*18*, *24*).

To move, the outer links rotated from being in parallel to being orthogonal with the center link. A nominal oscillation period lasted 10 s and involved 3 s of motion to transition to and from the U shape, interspersed with 2 s of pauses to allow the motor windings to cool. To protect the motor during entanglement, we implemented an overcurrent protection, such that the motor was turned off temporarily if the joint torque exceeded ~0.20 N·m.

Modules could move collaboratively through physical interactions; however, modules in isolation situated on a smooth, level surface had limited ability to self-locomote (Fig. 2D). Isolated modules moved comparably on either side of their body when placed on a level whiteboard surface. Across experiments with 10 independent modules actuated for 180 cycles, the average linear velocity was 0.240 ± 0.040 BL per cycle on side 1 and 0.245 ± 0.046 BL per cycle on side 2. The corresponding angular velocities were 0.009 ± 0.263 rad per cycle on side 1 and -0.099 ± 0.312 rad per cycle on side 2. No statistically significant side-dependent differences were observed in linear velocity (Wilcoxon signed-rank test, $P = 0.375$; paired Cohen's $d = 0.09$) or angular velocity ($P = 0.770$; $d = 0.05$). These measurements indicated weak net locomotion, consistent with slight asymmetries in mass distribution, multipoint ground contact, and small variations in contact friction between the two sides. This method of producing motion is similar to how bristle bots or vibrobots move, relying on asymmetric contact to rectify otherwise symmetric motion (*25*).

Intrinsic entanglement and motility

We used a comparative approach to analyze the "intelligence" that emerged from local mechanical interactions in the cross-link collective. Specifically, we showed that mechanical responses could drive adaptive behaviors (such as the emergence of stable chain configurations and phase drifting) that promoted cohesion and enhanced collective motility.

To study cross-link collective behaviors, we ran 10 trials where 10 modules were started in a pile on a level whiteboard surface. Although the modules quickly spread out to interact predominantly in two dimensions, the 3D pile served as a randomized initialization that naturally generated diversity in bonding configurations.

The contact dynamics of the oscillating modules quickly caused them to disperse beyond interaction range, at which point the modules moved independently without notable changes in direction (Fig. 3A). As modules lost mechanical contact with others, their motion became slow and consistent. Mean square displacement analysis revealed that they exhibited predominantly ballistic behavior (their behavior scaled linearly with time), and we observed predominantly chain sizes of one (Fig. 3, B and C).

To promote entanglement, we added two strips of VELCRO on both sides of each outer link (detailed in Materials and Methods

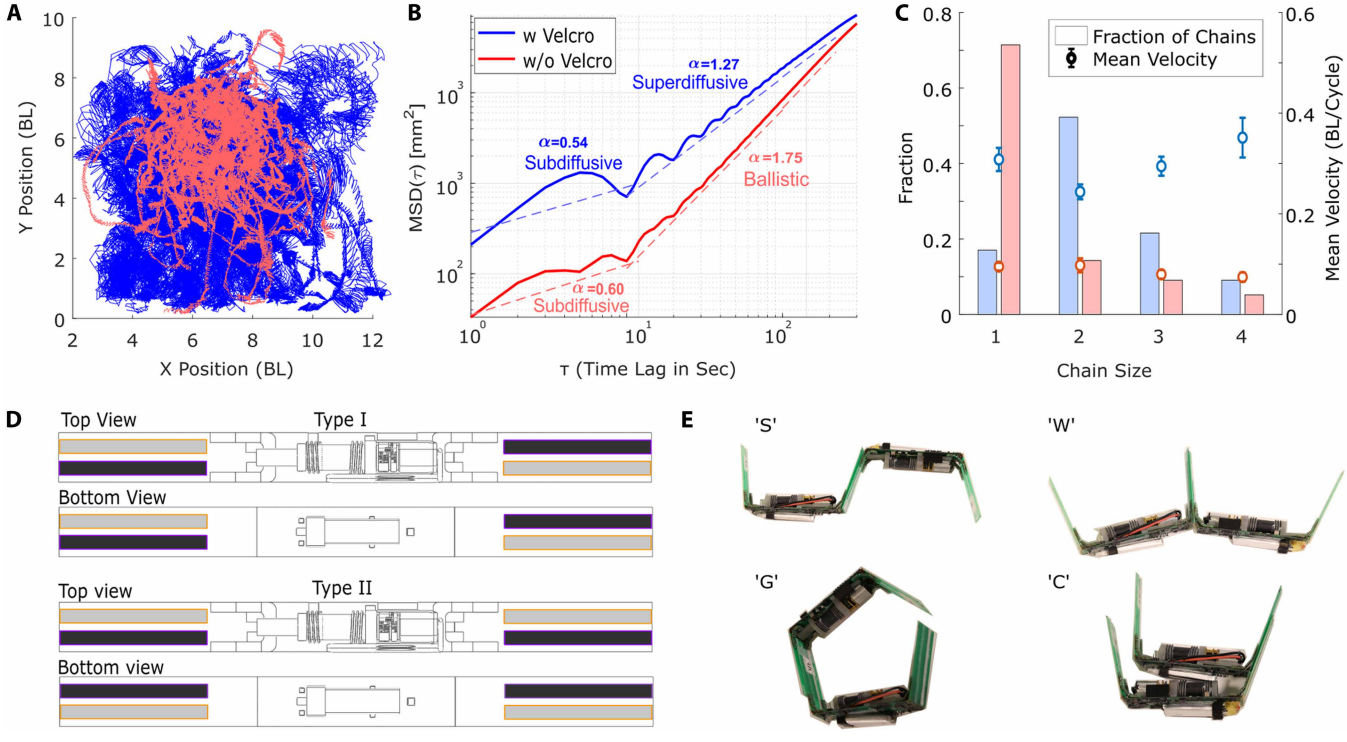

Fig. 3. Global behaviors with and without intermodule attraction. The graphs in (A) to (C) were generated using automated computer vision analysis on recorded experiments, in which 10 modules interacted mechanically on a flat surface for roughly 120 oscillation cycles, with 10 repetitions each. (**A**) Superimposed trajectories of modules with (blue) and without (red) VELCRO showing that modules capable of cross-linking travel further. (**B**) Mean square displacement (MSD) plot for modules with (blue) and without (red) VELCRO. Dashed lines represent power-law fits of the form $\mathrm{MSD}(\tau) \propto \tau^{\alpha}$ to visually indicate different transport regimes. (**C**) Normalized distribution of chain sizes and their mean velocities with (blue) and without (red) VELCRO capped at a chain size of four. Error bars denote SD ($n = 10$). (**D**) The cross-link collective consists of two types of modules, differentiated by their placement of VELCRO hook (dark blue) and loop (light gray) strips. (**E**) Four configurations in which two modules with VELCRO can cross-link.

and Fig. 3D). In contrast with magnetic or mechanical latch connections commonly used in modular robots, VELCRO provided asymmetric bonding: Modules engaged readily through incidental shear contact, whereas separation required stronger peel forces. In addition, the hook-loop structure enabled gradual, probabilistic bond formation and release, akin to the heterogeneous and transient cross-linking dynamics observed in active gels. Given the VELCRO placement, two modules could form "S," "W," "G," or double-nested "C" configurations (Fig. 3E and the "Possible configurations between two modules" section of Supplementary Materials and Methods). Building on these, chains of 2 to 10 modules could arrange in hundreds of different configurations. As we continued to analyze chain and material performance, we distinguished between "entanglement," similar to physical cross-links in polymers that are formed by proximity and mechanical interactions, and "cross-linking" caused by VELCRO bonds, which, similar to chemical cross-links in gels, were considerably stronger and formed a subset of the entanglement.

Repeating the same experiment, we found that the collective exhibited predominantly superdiffusive properties (the mean square displacement increased faster than linearly with time); cross-linked modules moved faster but exhibited more rotation than modules in isolation. The VELCRO caused substantially more cohesion (Fig. 3C); over the 10 trials, we found only 15 isolated modules compared with 55 for the modules without VELCRO. Examples experiments are provided in movie S3.

As expected, different types of chains formed in these experiments, ranging in size from 1 to 10 modules (Fig. 3C). For both entanglement and cross-linking, chains of two and three modules accounted for ~80% of all chains. Whereas these chains grew throughout the experiments, none broke. In entangled chains, we found that two- and three-module chains also persisted longer than bigger chains (see the "Motion over level surfaces" section of the Supplementary Materials and Methods). Purely on the basis of the VELCRO logic, S, G, and C configurations were twice as likely as W configurations. However, in accumulating all two-module chain data from the 10 trials (20 samples), we found that cross-linked S configurations were the most prevalent (13 of 20), followed by W (4 of 20) and G configurations (3 of 20), with no C configurations.

To explain these results, we modeled the locomotion properties of the S, W, and G configurations using resistive force theory (RFT). As previously demonstrated, RFT-based models could be applied in regimes where the coasting number (a dimensionless quantity characterizing the role of inertia in terrestrial locomotion) was less than one (*26*). In this regime, dynamics were dominated by internal shape changes, and inertial effects could be ignored. Our modules had a coasting number of ~0.001, which enabled us to borrow insights from theoretical and experimental studies in low–coasting-number locomotion strategies, especially related to the similarity between S-shaped configurations and multilink swimmers (*26*, *27*). In the low-coasting RFT-based model, we assumed quasistatic locomotion governed by instantaneous force and torque balance under Coulomb friction. Further details on the model are provided in the "Numerical simulation of system torque" section of Supplementary Materials and Methods. Using this framework, we investigated two key observations from our experiments: first, the predominance of S configurations over other configurations such as W and, second, the emergence of phase drift in S configurations.

Toward the first observation, we hypothesized that the VELCRO bond in the W configuration was more prone to breaking compared with the S configuration, resulting in a predominance of S-shaped configurations. To test this hypothesis, we numerically computed the minimum cohesion torque required from the Velcro bonds to maintain structural integrity during shape transitions. As illustrated in Fig. 4Ai, we analyzed a W configuration and identified the instantaneous torque τ_v that had to be resisted by the VELCRO connection to preserve cohesion. We calculated τ_v as a function of time and defined τ_{max} as the peak torque encountered during the motion cycle. For the chain to remain intact, the VELCRO had to provide torque resistance greater than τ_{max}. We then compared τ_{max} across W-, G-, and S-shaped configurations and found that W-shaped chains required notably higher torque to remain assembled, as shown in Fig. 4E. This increased mechanical demand likely contributed to the lower frequency of W-shaped configurations observed in experiments and might explain the dominance of the mechanically more stable S-shaped chains. In addition, on the basis of prior work on multilink swimmers (*26*, *28*), we noted that elongated, streamlined configurations such as the S tended to exhibit more efficient locomotion than more complex, appendage-rich forms such as the W configurations. Examples of the motion of S, W, G, and C configurations are provided in movie S4.

To address the second observation, we hypothesized that the built-in response to motor overtorque induced phase drift in the S configurations. Specifically, we calculated the instantaneous torques on the motorized joints (τ_1 and τ_2 in Fig. 4Bi) during shape change. Because a single motor was used to actuate both joints, we define the total motor torque as $\tau_m = \tau_1 + \tau_2$. We computed τ_m as a function of time (Fig. 4Bii) and empirically found that the peak motor torques required approached the physical torque limits of the module actuators. As described in the "Module design" section, this torque overload triggered a pause in the oscillation cycle to protect against overcurrent draw, inserting a delay of ~0.4π (or 2 s) in phase space. These pauses resulted in gradual phase drift in the module chain (illustrated in Fig. 4C). To test the model predictions, we numerically simulated phase drift arising from stall responses to overtorque (see the "Numerical simulation of system torque" section of Supplementary Materials and Methods). The resulting model-predicted phase-drift distribution (fig. S6) was qualitatively similar to the experimental results (Fig. 4F).

Modeling the peak torque of the S configuration as a function of intermodule phase lag (Fig. 4D) revealed that such phase drift might help reduce the required peak torque. In our experimental setting, modules were started upon hearing an audible signal, roughly with zero phase lag. High motor torque was typically required at small phase lags (for example, around 0.1π), which could induce delayed action responses. Consequently, the leading module experienced a phase delay, shifting the phase response from ~0.1π to −0.3π, which in turn reduced the motor torque demand. Furthermore, as noted in prior work (*28*), phase drift in the S configuration, similar to that in multilinked swimmers, actually enhanced locomotion performance, a phenomenon commonly observed in the undulatory slithering behavior of snakes. This suggested that what might initially have appeared as a failure mode could instead serve as an adaptive mechanism to alleviate excessive internal stresses.

Our experimental data agreed with the model predictions on how displacements and torque were affected by phase lag in two-module chains. We tracked and labeled the phase lag of all S configurations over the 10 experiments. Although all modules started synchronized upon detecting an audible signal, over time, the phase

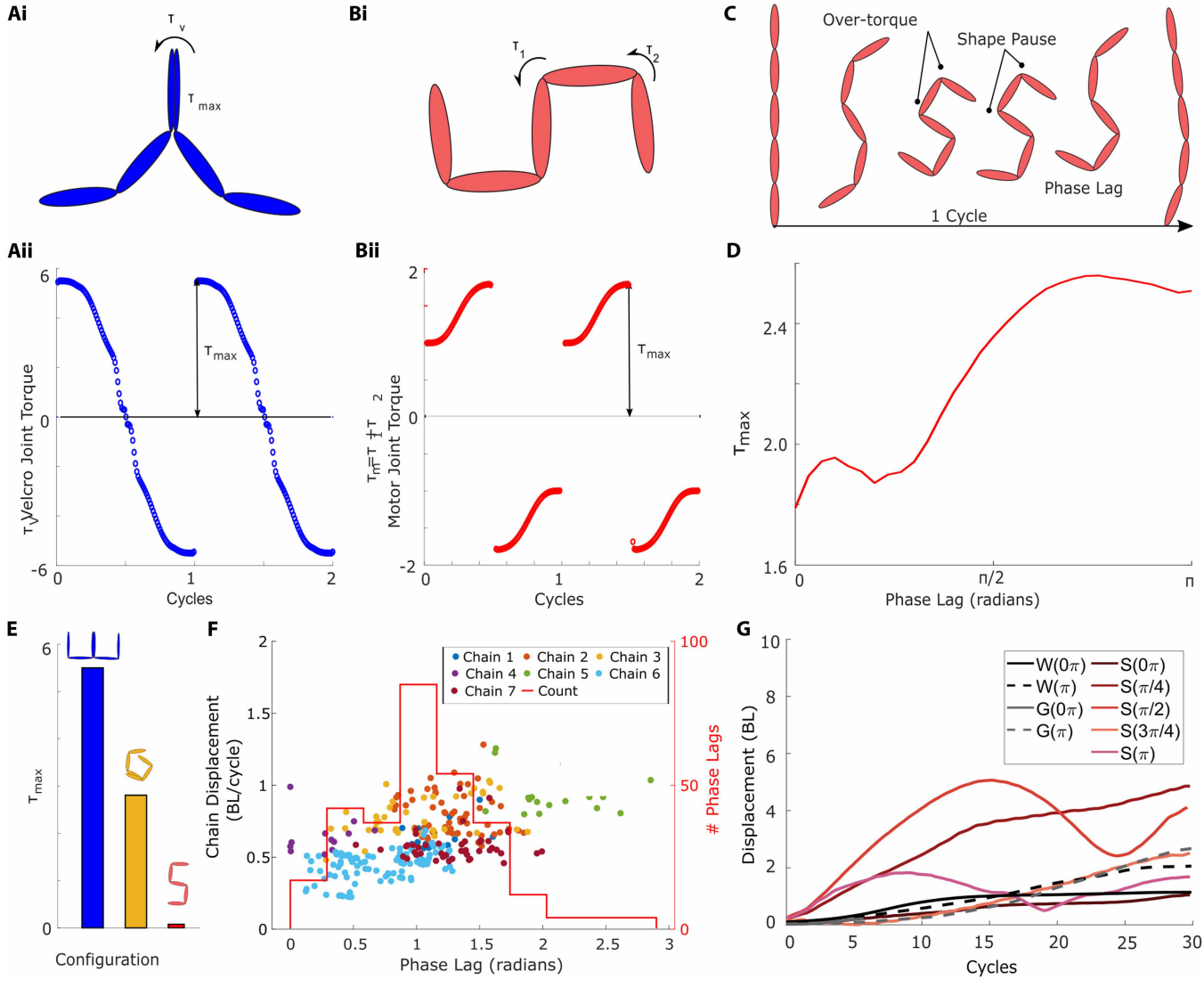

Fig. 4. Torque experienced by modules in chains depends on their configuration and phase lag. (**A**) (i) Illustration of VELCRO joint torque (τ_v) required to maintain the W configuration. (ii) Model-predicted τ_v as a function of time over two oscillation cycles. (**B**) (i) Illustration of motorized joint torques (τ_1 and τ_2) in the S configuration. (ii) Predicted overall motor torque ($\tau_m = \tau_1$ and τ_2) as a function of time. (**C**) Illustration of how torque overload induces motor delay, leading to intermodule phase drift. (**D**) Model prediction of maximum motor torque in S configuration as a function of intermodule phase offset. (**E**) Model-calculated maximum VELCRO joint torques across W, C, and S configurations, showing higher torque demand in W configurations. (**F**) Recorded phase lags between modules in S configurations from 10 repetitions of the experiment with 10 modules with VELCRO on a flat whiteboard surface. (**G**) Displacement magnitude from isolated runs with S, W, and G configurations under different actuation phase offsets over 30 oscillation cycles, with all trajectories referenced to their initial positions.

lag between modules in the chains changed, with a majority around π/3 (Fig. 4F). As predicted by the model, we also observed that motion was strongly influenced by the phase lag, especially in the S configuration. Figure 4G shows the displacement magnitude of isolated two-module chains over 30 oscillation cycles. In these experiments, two modules were initially placed in close proximity and allowed to cross-link naturally. In the S configuration, smaller phase lags (near π/4) yielded substantially larger net displacement, whereas larger phase lags (near π/2) also produced large displacement but were associated with helical, circling trajectories. In contrast, W and G configurations exhibited weaker sensitivity to phase lag.

To cross-validate our model predictions regarding chains in the W configuration, we conducted an additional set of nine experiments using these chains in isolation. Same as before, two modules were first placed in close proximity and allowed to cross-link naturally. They were then activated with a fixed phase offset, including four experiments with 0π phase offset, two with π/2 phase offset, one with 2/3π phase offset, and two with π phase offset. We found that three of these chains broke on their own after 5, 18, and 56 oscillations with 2/3π, 0π, and π phase lag, respectively. Although there was no trend in which chains broke, the fact that three of the nine broke within 56 oscillations aligned with the model prediction that W configurations experienced higher joint torques than G and S configurations. In terms of displacement, W configurations with π phase lag moved slower than the others (4.9 mm/s ± 0.46 mm versus 8.6 mm/s ± 1.0 mm). For more details on the W configurations, refer to the

"Two-module chains in W-configuration" section of Supplementary Materials and Methods. Repeating these trials for G configurations, we similarly observed a strong dependence of motion on phase lag (6.2 mm/s for 0π versus 8.0 mm/s for π; see further details in the "Two-module chains in G-configuration" section of Supplementary Materials and Methods.

In summary, our modeling and experiments revealed how physical chain configurations and phase dynamics influenced the stability and effectiveness of locomotion in the cross-link collective. S configurations dominated because of their lower cohesion torque requirements and higher motility. Phase drifting, which emerged from internal torque limits, served not as a failure mode but as an adaptive mechanism that enhanced performance. These findings highlighted how stochastic mechanical interactions alone could give rise to emergent, self-stabilizing behaviors that supported both cohesion and collective transport.

Entanglement and motility in the presence of external forces

Directed motion is critical for robot collectives to perform actual work. However, in systems composed of simple modules that depend on mechanical contacts for motility, the motion of the module itself may lead to dispersal and in turn hinder the mechanical interactions that cause further motion. By acting as an active gel where the polymer chains entangle, a collective can translate cohesively in the presence of an external directed force while exhibiting the necessary viscosity to prevent jamming when encountering obstacles. To study this phenomenon in our cross-link collective, we investigated motion and entanglement on a whiteboard with a 5° incline, just steep enough for isolated robots to be able to make some progress but not so much that they would roll when in their I shape.

The degree of cohesion and velocity in the force direction were related to the density of modules. To show this, we initialized a pile of 5, 10, 15, and 20 modules on the incline, tracking their trajectories and interactions over time (Fig. 5A and movie S5). We found that not only did a variety of entanglement and chain configurations occur in collectives at and larger than 10 modules but that the average velocity also dropped as the collective size grew beyond 15 modules because of congestion (Fig. 5, B and C). In addition, we observed that the number of modules for which progress on the incline stagnated increased with higher density, corresponding to an average of 0.9 ± 1, 3.4 ± 2.8, 4.7 ± 2.7, and 7.7 ± 2.3 modules for the 5, 10, 15, and 20 modules, respectively. These observations suggested a jamming-like reduction in mobility with increasing density, analogous to behavior reported in granular and active matter systems.

In other words, 10 modules reflected a balance inherent to the present system between the likelihood of forming productive chain configurations and the increased collisions and congestion that arose at higher populations. Although our experiments characterized how performance varied with density, the underlying dependence on more fundamental physical parameters, such as how motion depended on external and internal forcing, confinement, cross-link strength, and friction, remains to be fully understood and represents an important direction for future research. For the purposes of this study, all further experiments were conducted with 10 modules.

In addition to cohesion, these experiments showed that entanglement enhanced robustness to orientation. We observed a statistically significant difference between single modules ($n_1 = 245$) and chains ($n_2 = 78$) in terms of the directed velocity ($P = 0.0416$), defined as velocity in the direction of the force (Fig. 5D). We also found a statistically significant difference between single modules ($n_1 = 245$) and chains ($n_2 = 78$) in terms of their Euclidean velocity ($P = 0.00$). Although single modules had a mean directed velocity of 0.260 BL per cycle, 25% fell below 0.041 BL per cycle. In contrast, the lower quartile for modules in chains was below 0.848 BL per cycle. This difference occurred because single modules exhibited low orientation change and were, therefore, heavily dependent on their initial pose (Fig. 5E and movie S6). In contrast, chains tended to rotate notably more and were therefore less dependent on their current state (Fig. 5D). Consequently, although a single, well-aligned module might have traveled faster in isolation, entanglement improved overall cohesion and collective locomotion.

On the basis of experimental observations, we used RFT to model orientation robustness as a function of chain size. Specifically, we analyzed how chains of varying sizes and orientations responded to external forces. In our model, the external force was represented by the gravitational component acting on an incline, with magnitude given by $G\tan(\theta)$, where G is the gravitational force on the robot and θ is the slope angle. To generalize across different frictional conditions, we defined a dimensionless parameter $\tan(\theta)/\mu$, where μ is the friction coefficient.

As documented in (*29*), a shape-changing robot subjected to a constant external force will exhibit an additional response velocity, where the magnitude of this velocity is almost proportional to the external force. In this section, we computed how a single robot (Fig. 5F) and a chained robot (Fig. 5G) responded to such external forces under different orientations. Specifically, we considered two cases: parallel orientation (red curve) and perpendicular orientation (blue curve). Our results showed that the response velocity of a single robot was highly sensitive to orientation, with an up to 100% difference in speed between the parallel and perpendicular configurations. In contrast, chained modules exhibited substantially improved robustness to orientation, maintaining more consistent performance regardless of direction.

Drawing from the behavior of active gels that can deform, flow, and reconfigure around obstacles, we next demonstrated that the motion and cohesion of the cross-link collective persisted in the presence of obstacles (Fig. 6, A and B). We used an obstacle field composed of three rows of circular rods, each slightly bigger than the enclosed span of the U shape to prevent trapping modules. The obstacles were spaced apart slightly less than the full length of an I-shaped module to investigate the risk of jamming. We found that in the absence of obstacles, single modules dominated. However, as the collective encountered obstacles, it slowed down and increased the rate of entanglement (Fig. 6C). As the collective passed through the obstacle field, some of the chains broke, effectively preventing jamming; after they had passed, we observed that the fraction of single modules and smaller chains increased. When examining the continuous transition matrices without and with obstacles (Fig. 6D), we found that longer chains were more likely to break in the obstacle field. Similar results were seen in the experiment shown in the "Collective motion through a planar funnel" section of Supplementary Materials and Methods and movie S2, where the collective passed through a planar funnel.

Essentially, the collective exhibited viscous behavior upon encountering obstacles. Initially, the obstacles encouraged entanglement, but eventually, chains broke to prevent jamming. This behavior exemplified physical intelligence, in that it was inherent to the gel

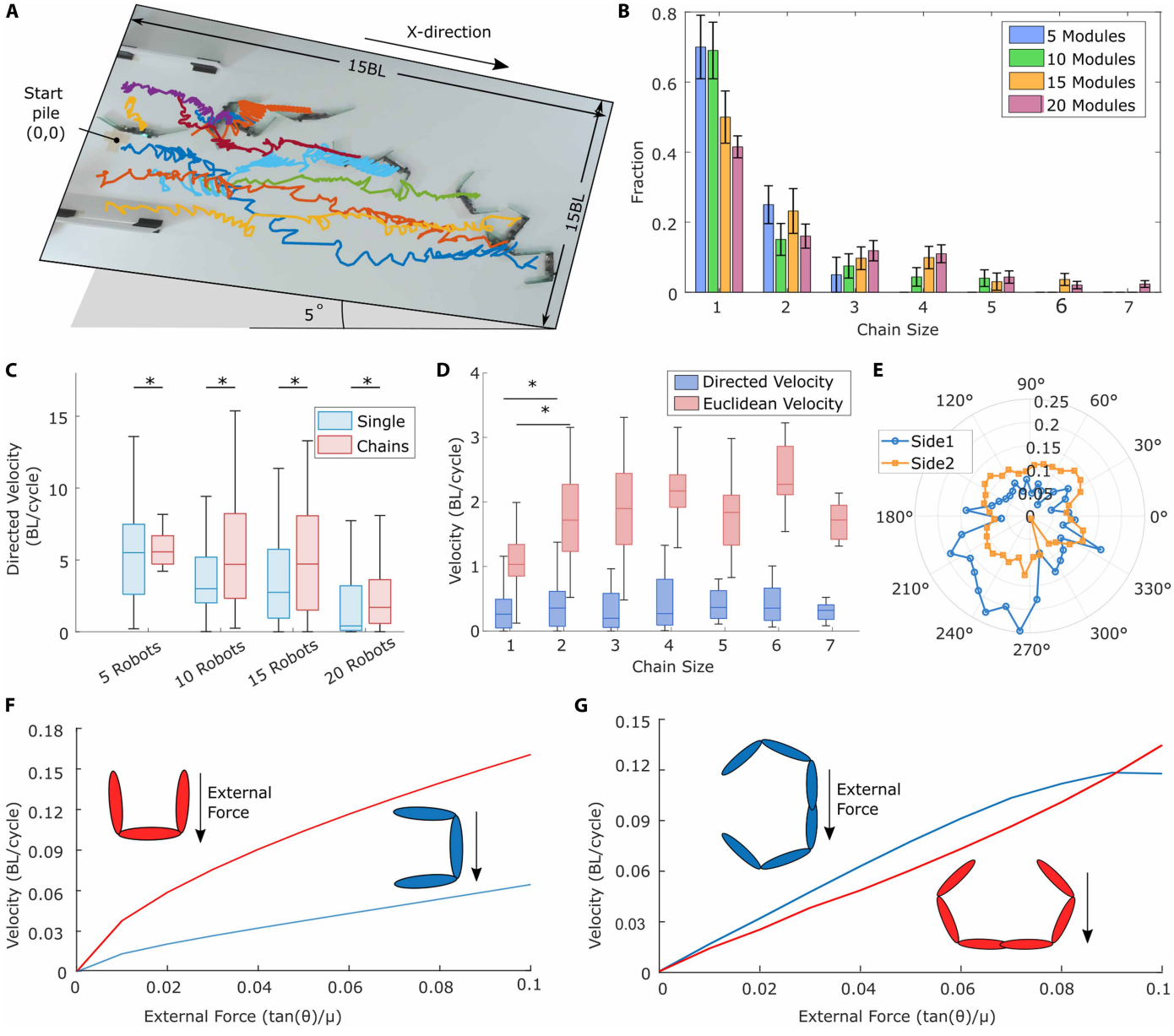

Fig. 5. Collective and individual behavior when exposed to an external force. (**A**) An example of trajectories of 10 modules on an incline; colors indicate individual paths. (**B**) Normalized distribution of chain sizes given different collective sizes. Error bars denote SD ($n = 40$). (**C**) Directed velocity (x direction) for a single module versus chains in experiments with different collective sizes. Data were derived from the difference between the average location of all modules in chains between video frames and smoothed with a moving mean of one oscillation cycle (10 s). Error bars denote SD ($n = 10$). (**D**) Directed and Euclidean velocity versus chain size across all experiments. Error bars denote SD ($n = 40$). Chain sizes greater than seven were excluded because of low frequency of occurrence. (**E**) Motion of a single module versus its orientation and rotation with respect to the x direction. (**F** and **G**) Effect of module and chain orientation on velocity.

and caused by transient cross-linking and highlighted the advantage of gel-like robotic substances over modules that are enclosed in fixed boundaries or permanently linked. In the next section, we discuss a simple, distributed control scheme to enhance entanglement, which was especially important to the cohesion of the collective in the absence of obstacles.

Cognizant entanglement and motility

When the cross-link collective followed a directed force, isolated modules that did not initially entangle could be left behind, especially if there were no physical hindrances that helped slow down the chains. This is problematic because real-world environments are characterized by frictional heterogeneity, which can disrupt cohesion and hinder the persistence of collective motion. Here, we showed that a simple, reactive, distributed control mechanism can address this problem, further promoting cohesion.

Our controller was based on the observation that chains typically moved faster on inclines than isolated modules; therefore, modules that were cognizant of their neighborhood could take measures to catch up if isolated. The controller was implemented as a finite state

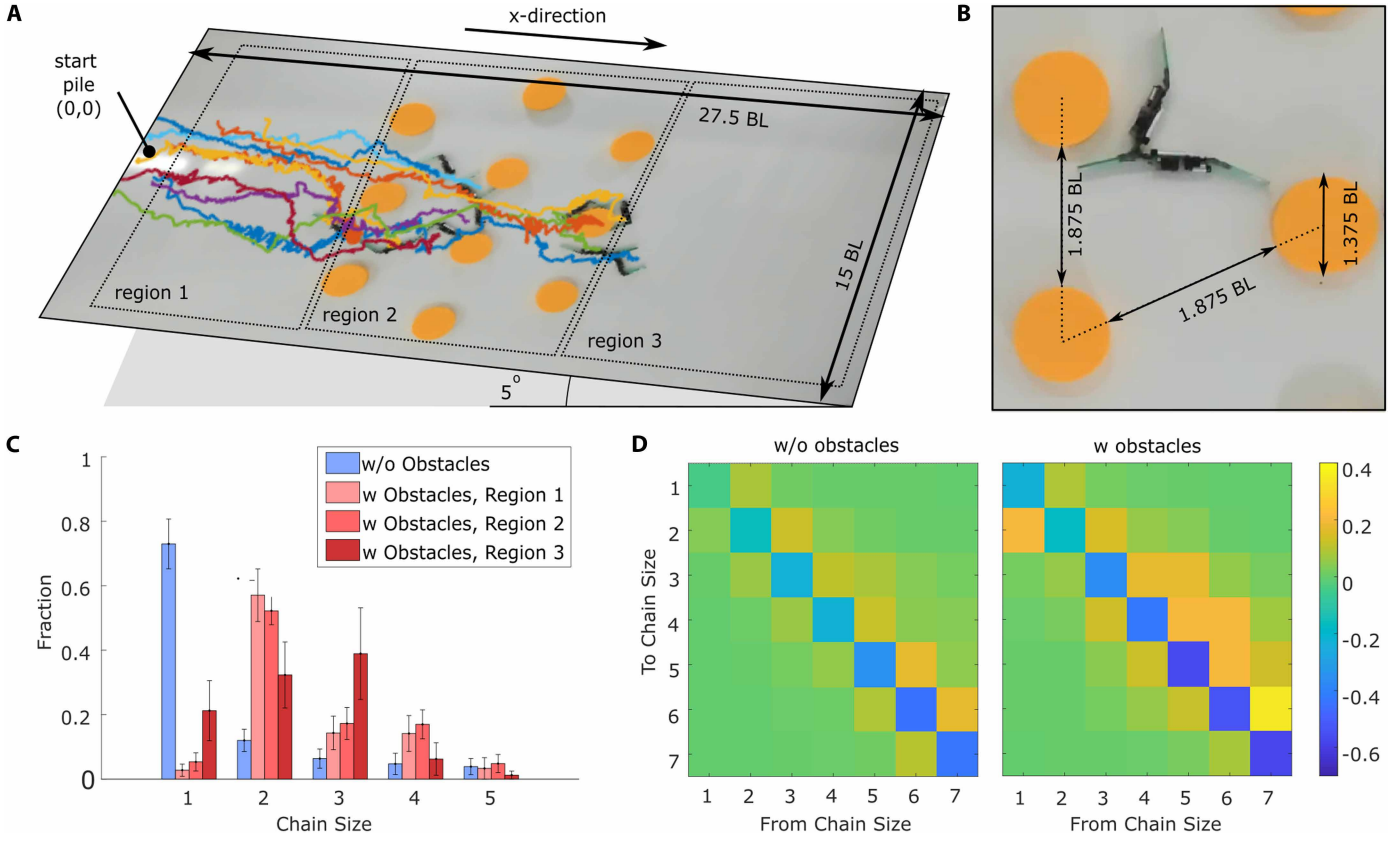

Fig. 6. Collective behavior when exposed to obstacles and an external force. (**A**) Example of trajectories of 10 modules on incline. Note that although the color spectrum overlaps with that of Fig. 5A, the modules are not the same. Regions 1 to 3 indicate before, in, and after the obstacle field, respectively. (**B**) Obstacle field dimensions with respect to the module BL. (**C**) Normalized distribution of chain sizes within regions and without obstacles. The bars show the mean of 10 experiment repetitions. Bars and error bars represent the mean and SD across repetitions ($n = 10$), respectively. (**D**) Continuous time transition rates for chains of different size on inclines without and with (region 2) obstacles.

machine operating independently on each module (Fig. 7A). In the default active state, modules oscillated at a nominal speed. If a module detected that it was isolated, then it emitted a close-range audible distress signal and sped up its oscillations. Modules that detected entanglement slowed down, and those that heard a distress signal halted their motion and propagated the signal. After a fixed duration, all modules reverted to their default active state. In effect, although the collective typically behaved similar to an active gel, this controller permitted localized neighborhoods to temporarily solidify when cohesion dropped, enabling isolated modules to catch up. An example of this behavior is provided in movie S7.

Each nominal oscillation cycle consisted of 3 s of motion (I to U), a 2-s pause, a 3-s motion (U to I), and 2-s pause. To modulate speed, isolated modules reduced their pauses to 0.5 s, whereas entangled modules extended pauses to 5.5 s. Because the modules shared a single supply rail, sensing during motor activity was unreliable; as such, sensor data were gathered throughout pauses and evaluated at the end of each full oscillation cycle, which was also when state transitions occurred. To detect entanglement, modules used their onboard accelerometers to monitor pitch (rotation around their longitudinal axis). Sudden pose changes that were not self-induced were interpreted as evidence of contact with other modules. The distress signal was implemented using the buzzer-microphone pair and could be detected up to 2.5 BL away.

We found that cognition significantly decreased the fraction of single modules in the collective, both on obstacle-free inclines and after passing through an obstacle field (Fig 7B and movie S7). On an obstacle-free incline, the fraction of single modules was lower with control (median = 0.78, $n = 9$) than without control (mean = 1.75, $n = 6$; two-sample t test, $P = 0.0274$). In addition, the number of modules that stagnated on the obstacle-free incline was lower with control (mean = 1.4 ± 1.5) than without control (mean = 3.4 ± 2.8). After clearing an obstacle field, the fraction of single modules was also lower with control (mean = 0.200, $n = 5$) than without control (mean = 0.318, $n = 5$; two-sample t test, $P = 0.0281$). Again, the number of modules that stagnated on the incline in the presence of obstacles was lower with control (mean = 2 ± 1.6) than without (mean 4 ± 0.7). As was expected, the best cohesion was achieved when collectives with cognition also encountered obstacles. In analyzing the transition rates, we observed that cognition had little influences on the longer chains but boosted the transition rate out of one-length chains. The transition rate from chain size 1 to 2 was 0.18 per second higher with control than without. This minimal form of distributed reactive control enabled modules to react to fracture and locally trigger cohesion, demonstrating how properties could be enhanced by using explicitly programmed intelligence on top of the mechanical intelligence that was inherent to the system.

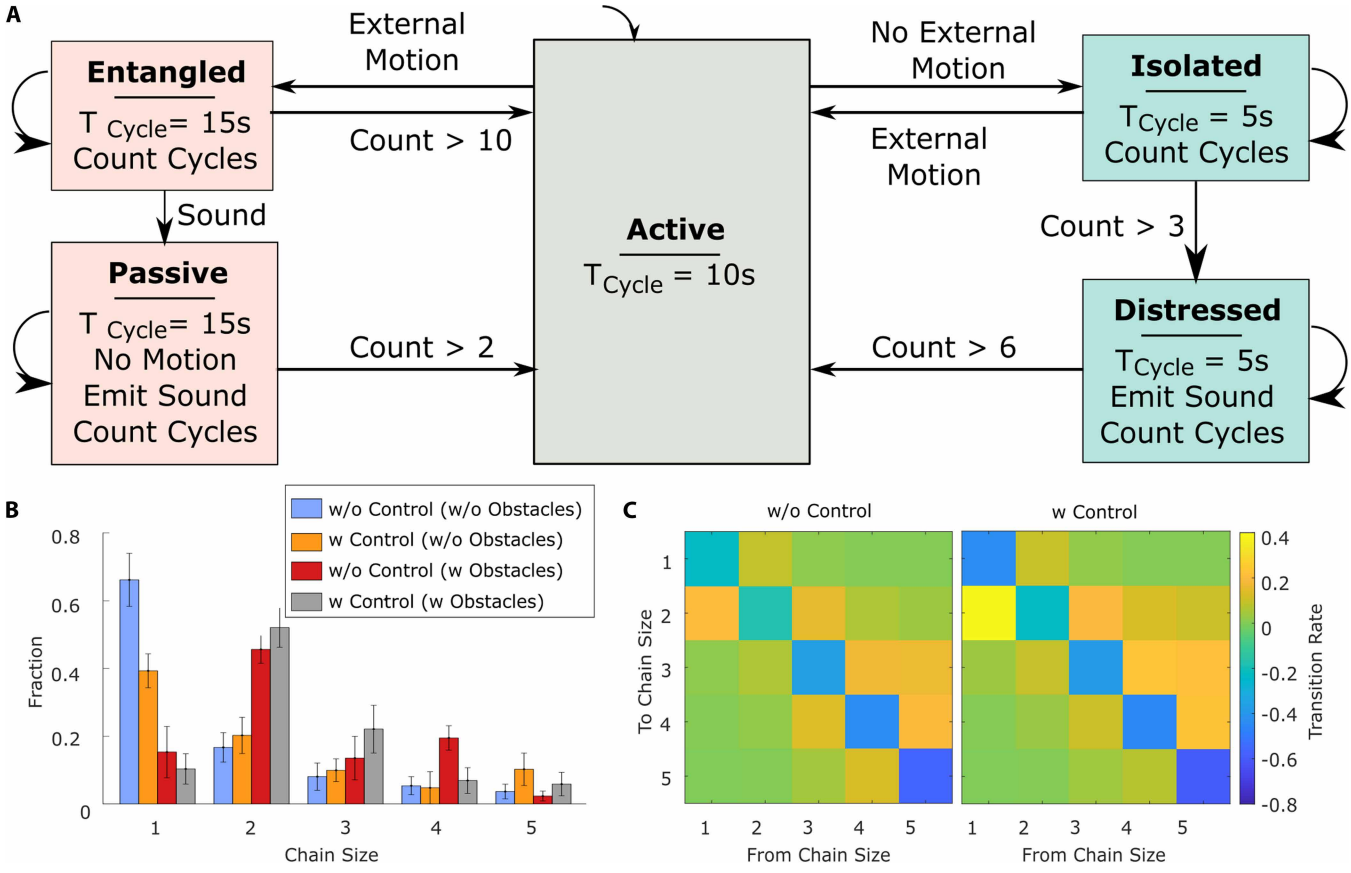

Fig. 7. Collective behavior with cognizant modules. (**A**) Logic flow chart of the decentralized control algorithm. Modules used local sensing to detect entanglement and isolated neighbors, triggering state changes to maintain or improve collective cohesion. (**B**) Normalized distribution of chain sizes with or without cognizant control in open or obstructed environments. Data were accumulated from all trials across the entire experimental arena. Bars and error bars represent the mean and SD, respectively, across repetitions ($n = 10$). (**C**) Continuous transition matrices without or with control, capped at a chain size of five.

Error tolerance

Because the cross-link collective outsourced topology to physical interactions, it inherently tolerated individual module failures, sensing noise, and fabrication variability. Across all incline experiments, 29 of the 650 deployed modules (~4% per trial) ceased shape-morphing, primarily because of depleted batteries or minor hardware faults. However, the collective remained functional: Failed modules were either carried along in chains or left behind without disrupting group-level motion.

Sensor noise was accommodated in a statistical sense, with classifications biased toward correct outcomes. Accelerometers used to detect entanglement produced signals that were dominated by fluctuations, yet by applying simple windowed variance thresholds, modules were able to distinguish between isolation and chain membership with high accuracy when evaluated over repeated cycles. Audible distress signals, implemented via low-cost microphone-buzzer pairs, were likewise detectable despite noise, enabling isolated robots to recruit neighbors without expensive spectrum analysis.

Last, despite fabrication variability, intermodule differences in motor current and sensing remained smaller than the intrinsic noise of the sensors themselves. This highlights an important feature of entanglement-based collectives: Functionality emerged from transient mechanical connections and redundant interactions rather than precise calibration of individuals. Together, these results, further detailed in the "Tolerance to faults, noise, and fabrication variance" section of Supplementary Materials and Methods, showed that the cross-link collective not only sustained motion under module failure but also maintained cohesion despite noisy sensing and imperfect fabrication, underscoring the robustness and graceful degradation that mechanical intelligence affords.

DISCUSSION

Robot collectives that exploit loose physical connections among homogeneous components with minimal sensing, communication, and control are increasingly relevant to applications in unstructured, dynamic settings and as model systems for soft-matter physics. Our work contributes to this growing class of robots, demonstrating that transient entanglement (akin to cross-linking in active gels) can promote emergent cohesion, resilience, and adaptive response to environmental barriers. In contrast with recent demonstrations of locomotion by dense, permanently entangled robot "blobs," our cross-link collective achieves self-organized cohesion and locomotion through transient entanglement.

A central result of this study is that such interactions allow modules to form chains that enhance both cohesion and locomotion. These chains mechanically adjust their configuration and phase lag in response to internal strain and external constraints. In particular,

we show that specific chain configurations are not only more mechanically stable but also more efficient and resilient in motion. These dynamics are reminiscent of active gels where local entanglement dictates macroscopic behavior, and they underline the power of mechanical intelligence in shaping collective responses.

The adaptive nature of these chains is further highlighted when subjected to external forces and obstacles. Rather than jamming or dispersing, the collective transitions to a viscous-like state by breaking and reforming chains, effectively flowing around impediments. This response arises naturally from mechanical intelligence, not from planning or deliberation. We further show that a simple, reactive controller, based on proprioceptive state estimation and local stalling, is sufficient to enhance cohesion, demonstrating a minimal form of distributed computational intelligence that complements the system's mechanical intelligence.

Such cohesive behavior, emerging from transient and unstructured connections, contrasts with classical modular robot systems that rely on fixed topologies and tightly coordinated behaviors. By avoiding permanent bonds and instead embracing weak, reversible links, our cross-link collective achieves greater flexibility, redundancy, and fault tolerance. Our system remains functional even with partial failures, noisy sensors, and misaligned modules, highlighting the robustness and graceful degradation that mechanical intelligence affords. These findings align with cohesion strategies observed in biological systems, from fungus and mussels to worms and fire ants, where entanglement and physical clustering enable collective behaviors and survival under uncertainty.

This minimalistic approach also offers practical benefits. It reduces cost, simplifies fabrication, and scales more readily than high-bandwidth, sensor-heavy collectives, for example, offering a path toward future implementations of engineered active matter at micro- or nanoscale. Moreover, by mimicking the adaptable viscosity of active gels, cross-link collectives may serve as a blueprint for obstacle-resilient robot swarms, capable of reshaping and self-organizing in complex environments. In our experiments, whereas the robots primarily settled into planar motion, the use of 3D-initialized entanglement and designs optimized for volumetric interactions, suggesting further promise for fully 3D locomotion and task execution.

Building on insights from this study, future work may involve design modifications specifically to encourage more mobile two-module S configurations and adaptation of the motor current limit and control to optimize phase lag in chains. More broadly, we may explore how such collectives behave under multidirectional forces, in more rugged terrains, and with higher degrees of internal heterogeneity. Another promising avenue is to develop control strategies that dynamically regulate cohesion, such as to avoid congestion in crowded scenarios, allowing the collective to transition between aggregation, dispersion, and preferred chain lengths through context-dependent tuning of the oscillation period, phase lag, and connection topology. Key questions are how mechanical intelligence scales with complexity, both in terms of module number and interaction diversity, and how simple local rules and morphological features can be composed into increasingly capable robotic matter.

MATERIALS AND METHODS

Study design

No formal power analysis was applicable to this study; instead, sample sizes were based on systematic characterization of collective performance with and without VELCRO, at different densities (5, 10, 15, and 20 modules), on inclines and in obstacle fields, and with or without control. Trials were run for predefined durations or until all modules reached the end of the arena, with no selective stopping. All completed trials were included in the analysis, including malfunctioning modules and modules that ran low on battery. Trajectories, module orientations, interaction events, and phase dynamics were quantified using overhead video tracking and image analysis as described in the following subsections.

The objective of this study was to investigate how passive VELCRO-mediated entanglement enables cohesive locomotion, adaptive reconfiguration, and robust collective behavior in a group of simple robotic modules. We examined how density influenced collective locomotion and chain characteristics, how the locomotion of chains compared with that of single modules, how joint torque affected phase relationships in two-module chains and the prevalence of different configurations, and how emergent chain formations responded to environmental interactions and simple decentralized controllers.

All experiments in this study were performed with multiple independent trials (typically 10), and the exact number of replicates for each experimental condition is reported in the corresponding figure legends and related text. Across all experiments, trials were treated as independent replicates.

Robotic modules

The cross-link modules, shown in Fig. 2 (A to C), were designed for scientific studies across robotics and experimental physics disciplines, with the primary objectives being to enable a high rate of entanglement compared with their Smarticle predecessors (*17*), to enable operation of large collectives, and to lower the barrier of entry for researchers across disciplines (*23*). The choice of materials catered to both module capability and platform accessibility in terms of simple, inexpensive, rapid manufacturing. The modules were composed of 19 printed circuit board (PCB) pieces and three 3D printed components. The three main links and the four-bar crank and slider mechanism were all composed of stiff FR-4 (fiberglass-reinforced epoxy resin), and the flexures between the links were composed of flex-PCBs (polyimide). To drive the outer links, we used a 298:1 micrometal motor from Pololu. The motor mounts and bearings were printed in a Formlabs 2.0 using Tough1500 resin, and the worm gears were printed in a Carbon3D printer with UMA90 resin. The holding and lifting strength of this mechanism were documented in previous work (*23*) and in the "Module lifting and holding force" section of Supplementary Materials and Methods. In that work, we also demonstrated the durability through 400 sequential motion cycles, although in practice, the modules used in this study have vastly outlasted this limit.

The center link, which came preassembled from a fabrication house, mounted the primary circuit and components. The microcontroller (an 8-bit ATmega328) facilitated low barrier of entry, similar to popular platforms in the do-it-yourself movement (*30*). Sensor modalities included a three-axis accelerometer, battery voltage, motor current, a rotational encoder, an infrared photo transistor, and a microphone-buzzer pair. These modalities were all documented in the original paper (*23*) and supported studies such as audio synchronization, light/audio-enabled motion, contact-based wave propagation, smart matter adaptive tensile and compression strength, and three-dimensional entanglement. An onboard 180-mAh, 3.7-V lithium polymer battery supported experiments up to 40 min in duration.

One of the outer links had an integrated coil that could be used to charge the battery wirelessly, lowering the time needed for hands-on involvement between experiments. Assembling a module took just 15 min. It involved fusing the boards and flexures via solder connections in an oven, after which the battery, motor, and 3D printed motor mounts could be press-fit on to the assembly. At a collective size of 100, a module cost $72, on par with the existing Smarticles and the popular Kilobots research platform (*31*).

To support module cross-linking, we added two thin strips of VELCRO to each side of each of the outer links on all robots. Each strip measured 6.5 mm by 60 mm. We used VELCRO brand Thin Clear with an estimated tensile strength of 0.21 N/cm^2 and a shear strength of 0.34 N/cm^2. For context, this meant that a good bond between two links would support the hanging weight of approximately one module. Practically, the strength varied depending on how well the links were aligned and how forcefully they interacted when they bonded.

Statistical analysis

All experiments were performed on whiteboard surfaces with controlled lighting and overhead camera (Logitech C920) recording at 30 frames/s. To extract the location of all modules in each video frame, we used the YOLOv8 Oriented Bounding Boxes (*32*) multi-object tracking in Python. We trained the YOLO network using 333 manually labeled frames in which the joints and tips of the two outer links of each module were marked.

The quantitative analysis of the extracted module and chain trajectories was performed in MATLAB. To generate module trajectories, we used a Hungarian algorithm to match module locations over consecutive frames and lastly performed a manual pass to ensure data validity. To extract entangled chain configurations and trajectories, we extracted appropriately sized visual blobs in each frame and matched them with module trajectories and identifiers to further generate chain analytics over time. Displacement data were normalized to BLs on the basis of the 80-mm module center body dimension. Because chains were identified visually, many of these chains occurred because of physical proximity, not VELCRO bonds. When applicable, cross-linked modules (modules connected via VELCRO) were tracked manually. To focus on the collective behavior after convergence, the first 30 s of every experiment was ignored. For the experiments on an incline, the first 0.2 m of the incline was also ignored. In addition, to suppress spurious effects, only chains that persist five or more cycles were used to generate the plots in Figs. 3 to 7. Experimental results are reported as means ± SD unless otherwise noted.

Supplementary Materials

The PDF file includes:
Materials and Methods
Figs. S1 to S9
Legends for movies S1 to S7
References (*33*, *34*)

Other Supplementary Material for this manuscript includes the following:
Movies S1 to S7
Data file S1

REFERENCES AND NOTES

1. N. J. Mlot, C. A. Tovey, D. L. Hu, Fire ants self-assemble into waterproof rafts to survive floods. *Proc. Natl. Acad. Sci. U.S.A.* **108**, 7669–7673 (2011).
2. Y. Ozkan-Aydin, D. I. Goldman, M. S. Bhamla, Collective dynamics in entangled worm and robot blobs. *Proc. Natl. Acad. Sci. U.S.A.* **118**, e2010542118 (2021).
3. W. Van Winkle Jr, Effect of environmental factors on byssal thread formation. *Mar. Biol.* **7**, 143–148 (1970).
4. H. Wang, J. Tao, Z. Wu, K. Weiland, Z. Wang, K. Masania, B. Wang, Fabrication of living entangled network composites enabled by mycelium. *Adv. Sci.* **11**, e2309370 (2024).
5. G. H. Koenderink, E. K. Paluch, Architecture shapes contractility in actomyosin networks. *Curr. Opin. Cell Biol.* **50**, 79–85 (2018).
6. J. Veenstra, C. Scheibner, M. Brandenbourger, J. Binysh, A. Souslov, V. Vitelli, C. Coulais, Adaptive locomotion of active solids. *Nature* **639**, 935–941 (2025).
7. B. Saintyves, M. Spenko, H. M. Jaeger, A self-organizing robotic aggregate using solid and liquid-like collective states. *Sci. Robot.* **9**, eadh4130 (2024).
8. M. R. Devlin, S. Kim, O. Campàs, E. W. Hawkes, Material-like robotic collectives with spatiotemporal control of strength and shape. *Science* **387**, 880–885 (2025).
9. W. Zeng, X. Ding, Y. Jin, B. Liu, R. Zeng, F. Gong, Y. Lou, L. Jiang, H. Li, Magnetic soft millirobot with simultaneous locomotion and sensing capability. *Npj Flex. Electron.* **9**, 59 (2025).
10. S. Ceron, G. Gardi, K. Petersen, M. Sitti, Programmable self-organization of heterogeneous microrobot collectives. *Proc. Natl. Acad. Sci. U.S.A.* **120**, e2221913120 (2023).
11. S. Li, R. Batra, D. Brown, H.-D. Chang, N. Ranganathan, C. Hoberman, D. Rus, H. Lipson, Particle robotics based on statistical mechanics of loosely coupled components. *Nature* **567**, 361–365 (2019).
12. N. J. Wilson, S. Ceron, L. Horowitz, K. Petersen, Scalable and robust fabrication, operation, and control of compliant modular robots. *Front. Robot. AI* **7**, 44 (2020).
13. S. Li, B. Dutta, S. Cannon, J. J. Daymude, R. Avinery, E. Aydin, A. W. Richa, D. I. Goldman, D. Randall, Programming active cohesive granular matter with mechanically induced phase changes. *Sci. Adv.* **7**, eabe8494 (2021).
14. W. Savoie, T. A. Berrueta, Z. Jackson, A. Pervan, R. Warkentin, S. Li, T. D. Murphey, K. Wiesenfeld, D. I. Goldman, A robot made of robots: Emergent transport and control of a smarticle ensemble. *Sci. Robot.* **4**, eaax4316 (2019).
15. C. Kaeser, J. Kwon, E. Challita, H. Tuazon, R. J. Wood, S. Bhamla, J. Werfel, "Individual and collective behaviors in soft robot worms inspired by living worm blobs" in *2025 IEEE International Conference on Robotics Automation (ICRA)* (IEEE, 2025), pp. 2577–2583.
16. J. E. Avron, O. Raz, A geometric theory of swimming: Purcell's swimmer and its symmetrized cousin. *New J. Phys.* **10**, 063016 (2008).
17. W. Savoie, A. Pazouki, D. Negrut, D. Goldman, "Smarticles: Design and construction of smart particles to aid discovery of principles of smart, active granular matter," paper presented at the First International Symposium on Swarm Behavior and Bio-Inspired Robotics, Kyoto, Japan, 29 October 2015.
18. W. Savoie, H. Tuazon, I. Tiwari, M. S. Bhamla, D. I. Goldman, Amorphous entangled active matter. *Soft Matter* **19**, 1952–1965 (2023).
19. W. Savoie, S. Cannon, J. J. Daymude, R. Warkentin, S. Li, A. W. Richa, D. Randall, D. I. Goldman, Phototactic supersmarticles. *Artif. Life Robot.* **23**, 459–468 (2018).
20. R. Warkentin, W. Savoie, D. I. Goldman, "Locomoting robots composed of immobile robots" in *2018 Second IEEE International Conference on Robotic Computing (IRC)* (IEEE, 2018), pp. 224–227.
21. W. Zhou, Z. Hao, N. Gravish, Collective synchronization of undulatory movement through contact. *Phys. Rev. X* **11**, 031051 (2021).
22. P. Chvykov, T. A. Berrueta, A. Vardhan, W. Savoie, A. Samland, T. D. Murphey, K. Wiesenfeld, D. I. Goldman, J. L. England, Low rattling: A predictive principle for self-organization in active collectives. *Science* **371**, 90–95 (2021).
23. D. Ma, J. Chen, S. Cutler, K. Petersen, "Smarticle 2.0: Design of scalable, entangled smart matter," in *Distributed Autonomous Robotic Systems: 16th International Symposium*, vol. 28 of *Springer Proceedings in Advanced Robotics* (Springer, 2022), pp. 509–522.
24. N. Gravish, D. Goldman, "Entangled granular media," in *Fluids, Colloids and Soft Materials: An Introduction to Soft Matter Physics*, A. Fernandez-Nieves, A. M. Puertas, Eds. (Wiley, 2016), pp. 341–354.
25. G. Cicconofri, A. DeSimone, Motility of a model bristle-bot: A theoretical analysis. *Int. J. Non Linear Mech.* **76**, 233–239 (2015).
26. J. M. Rieser, B. Chong, C. Gong, H. C. Astley, P. E. Schiebel, K. Diaz, C. J. Pierce, H. Lu, R. L. Hatton, H. Choset, D. Goldman, Geometric phase predicts locomotion performance in undulating living systems across scales. *Proc. Natl. Acad. Sci. U.S.A.* **121**, e2320517121 (2024).
27. T. Wang, C. Pierce, V. Kojouharov, B. Chong, K. Diaz, H. Lu, D. I. Goldman, Mechanical intelligence simplifies control in terrestrial limbless locomotion. *Sci. Robot.* **8**, eadi2243 (2023).
28. B. Chong, T. Wang, E. Erickson, P. J. Bergmann, D. I. Goldman, Coordinating tiny limbs and long bodies: Geometric mechanics of lizard terrestrial swimming. *Proc. Natl. Acad. Sci. U.S.A.* **119**, e2118456119 (2022).
29. B. Chong, J. He, S. Li, E. Erickson, K. Diaz, T. Wang, D. Soto, D. I. Goldman, Self-propulsion via slipping: Frictional swimming in multilegged locomotors. *Proc. Natl. Acad. Sci. U.S.A.* **120**, e2213698120 (2023).
30. A. Nayyar, V. Puri, "A review of Arduino board's, Lilypad's & Arduino shields" in *2016 3rd International Conference on Computing for Sustainable Global Development (INDIACom)* (IEEE, 2016), pp. 1485–1492.

31. M. Rubenstein, A. Cornejo, R. Nagpal, Programmable self-assembly in a thousand-robot swarm. *Science* **345**, 795–799 (2014).
32. A. B. Mitrev, G. Mirceva, "YOLOv8 Oriented Bounding Box (OBB) model for Waymo open dataset" in *ICT Innovations 2024. TechConvergence: AI, Business, and Startup Synergy*, B. Risteska Stojkoska, S. Janeska Sarkanjac, Eds., vol. 2436 of *Communications in Computer and Information Science* (Springer, 2025); https://doi.org/10.1007/978-3-031-86162-8_7.
33. R. Hartenberg, J. Danavit, *Kinematic Synthesis of Linkages* (McGraw-Hill, 1964).
34. R. Budynas, K. Nisbett, *Shigley's Mechanical Engineering Design* (McGraw-Hill Education, ed. 11, 2020).

Acknowledgments: We thank E. Garner and A. Anand for the help in early revisions of the platform and model. **Funding:** This work was supported by the National Science Foundation under grant nos. 2042411 and 1933284 and a Packard Fellowship for Science and Engineering.
Author contributions: D.M. designed modules, performed all experiments, and analyzed experimental data. B.C. designed the model and helped analyze data. All authors contributed to data interpretation and manuscript preparation. **Competing interests:** The authors declare that they have no competing interests. **Data, code, and materials availability:** All data needed to evaluate the conclusions in the paper are present in the paper, the Supplementary Materials, and in the database 10.5281/zenodo.18271890. No new materials were generated or used in this study.

Submitted 26 September 2025
Accepted 22 April 2026
Published 20 May 2026
10.1126/scirobotics.aec6393

Science Robotics

Cross-link collective: Entangled robotic matter with cohesive motion

Danna Ma, Baxi Chong, Daniel I. Goldman, and Kirstin H. Petersen

Sci. Robot. **11** (114), eaec6393. DOI: 10.1126/scirobotics.aec6393

Science Robotics (ISSN 2470-9476) is published by the American Association for the Advancement of Science. 1200 New York Avenue NW, Washington, DC 20005. The title *Science Robotics* is a registered trademark of AAAS.